

## Electronic Supporting Information (ESI)

### Understanding the molecular origin of solid-state emitting PMI realized via the detection of hazardous organic peroxides

Rupam Roy,<sup>a</sup> Rohit Bhowal,<sup>b#</sup> Vikas Sharma,<sup>a#</sup> Deepak Chopra<sup>\*b</sup> and Apurba Lal Koner<sup>\*a</sup>

<sup>a</sup> Bionanotechnology Lab, Department of Chemistry  
Indian Institute of Science Education and Research Bhopal  
Bhopal Bypass Road, Bhauri, Bhopal, Madhya Pradesh, INDIA  
E-mail: [akoner@iiserb.ac.in](mailto:akoner@iiserb.ac.in)

<sup>b</sup> Crystallography and Crystal Chemistry Laboratory, Department of Chemistry, Indian Institute of Science Education and Research Bhopal  
Bhopal Bypass Road, Bhauri, Bhopal, Madhya Pradesh, INDIA  
E-mail: [dchopra@iiserb.ac.in](mailto:dchopra@iiserb.ac.in)

# these authors contibuted equally to this work

## **Experimental Section**

The fluorogenic probe PMISS was synthesized according to our reported protocol.<sup>1</sup> The solvents toluene, tetrahydrofuran and 1,4-dioxane for the detection were purchased from commercial source like Sisco Research Laboratories (SRL), Thomas Baker and used as received without any further purification unless otherwise mentioned. All the peroxides have been purchased from Spectrochem and Tokyo Chemical Industry (TCI). For spectroscopic measurements with above mentioned peroxides, toluene was taken as solvent because of good solubility of PMISS and peroxides, as well as inert nature of toluene. To purify the compounds, silica gel (particle size 100-200 mesh) from Merck was used for column chromatography. <sup>1</sup>H NMR spectra were recorded using Bruker 500 MHz spectrometer. The chemical shifts of compounds peak were determined with respect to the residual solvent signal ( $\delta = 7.26$ ). Atmospheric pressure chemical ionization (APCI) mass spectrometry data were obtained using Bruker MicroTOF-Q-II mass spectrometer and chloroform was used as solvent.

## **Instrumentation**

### **Steady-state absorption and fluorescence measurements.**

Steady-state UV-Vis. Spectra were recorded using Perkin Elmer and Carry 5000 spectrophotometer from Agilent Technologies using quartz cuvette of 1 cm path length. The temperature-dependent absorption studies were performed using Analytik Jena Specord 200 plus UV spectrophotometer. The concentration of PMISS and OPs were maintained as mentioned in manuscript for effective transformation. For solid-state absorption study, sample was mixed with BaSO<sub>4</sub> and grinded effectively to make powder sample. The powder sample was poured in sample holder and measured the absorption of the solid sample in Carry 5000 spectrophotometer using diffusion reflectance method. The steady-state fluorescence measurement and kinetics were carried out by HORIBA Jobin Yvon Fluorolog and HORIBA Fluoromax using 1 cm path length quartz cuvette. For the fluorescence measurements, the excitation and emission slits were varied according to condition of measurements. Solid state emission spectra of BaSO<sub>4</sub> mixed sample was measured by keeping the holder at specific angle in Jobin Yvon Fluorolog.

### **Time-resolved fluorescence measurement.**

Fluorescence lifetime or time-resolved fluorescence measurement was carried out using time-correlated single photon counting (TCSPC) setup from a Hamamatsu MCP photomultiplier (R-

3809U-50). The 509 nm pico-second laser was used as excitation source for the lifetime measurements and photon-count was set up to 10,000. The instrument response function (IRF) was measured using a dilute suspension of Ludox (Sigma Aldrich) before starting the measurement. The emission polarizer was fixed at magic angle (54.7 °) with respect to excitation polarizer. The bi-exponential decay was determined by using deconvolution method in supplied software DAS v6.2. The fitting parameter (chi-square value ( $\chi^2$ )) is considered in the range from 0.9-1.2. Lifetime measurement by TCSPC was performed at room temperature (298 K).

### **Fluorescence Quantum Yield (QY) determination.**

- (i) **QY in solution:** Fluorescence quantum yield for both species were determined from the emission spectra in CHCl<sub>3</sub> by considering 2,6-diisopropyl perylene monoamide as reference.<sup>2</sup>
- (ii) **QY in solid-state:** Absolute QY of PMISSO<sub>2</sub> powder was measured using BaSO<sub>4</sub>-coated integrated sphere from HORIBA Jobin Yvon attached to Fluorolog. Powder sample was prepared by proper mixing of PMISSO<sub>2</sub> with BaSO<sub>4</sub>. Powder sample was excited at 517 nm and emission range was fixed in 527-800 nm region.

### **Infrared Spectroscopy.**

IR spectra was recorded for the compounds by preparing thin-films on KBr pellet.

### **Calculation of CIE chromaticity Index.<sup>3</sup>**

The CIE chromaticity Index of the solid state emissive PMISSO<sub>2</sub> was calculated by using the following equations:

$$X = \sum_{K=1} \Phi_K(\lambda) B_K(\lambda)$$

$$Y = \sum_{K=1} \Phi_K(\lambda) G_K(\lambda)$$

$$Z = \sum_{K=1} \Phi_K(\lambda) R_K(\lambda)$$

Where the Tristimulus values X, Y, Z represent a specific color in color coordinates.  $B_K(\lambda)$ ,  $G_K(\lambda)$ ,  $R_K(\lambda)$  are defined as color matching functions of a standard colorimetric observer.  $\Phi_K(\lambda)$ , spectral distribution of color stimulus obtained from the emission spectra of species. The CIE co-ordinates (x, y, z) was calculated by considering the equations:  $x = X/(X+Y+Z)$ ,  $y = Y/(X+Y+Z)$  and  $z = Z/(X+Y+Z)$ .

### Fluorescence microscopy image.

Fluorescence microscope image of red emitting crystal of PMISSO<sub>2</sub> was captured in OLYMPUS IX-83-inverted fluorescence microscope and the image was processed by OLYMPUS cellsens dimension 1.1 software.

### Differential Scanning Calorimetry (DSC).

The DSC traces of both PMISSO and PMISSO<sub>2</sub> were recorded in a PerkinElmer DSC 6000 instrument where approximately 1.0 mg of each compound were successively placed in hermetically sealed aluminium pan in vacuum and subsequently scanned at a rate of 3°C/min under a dry nitrogen purge (20 mL/min).

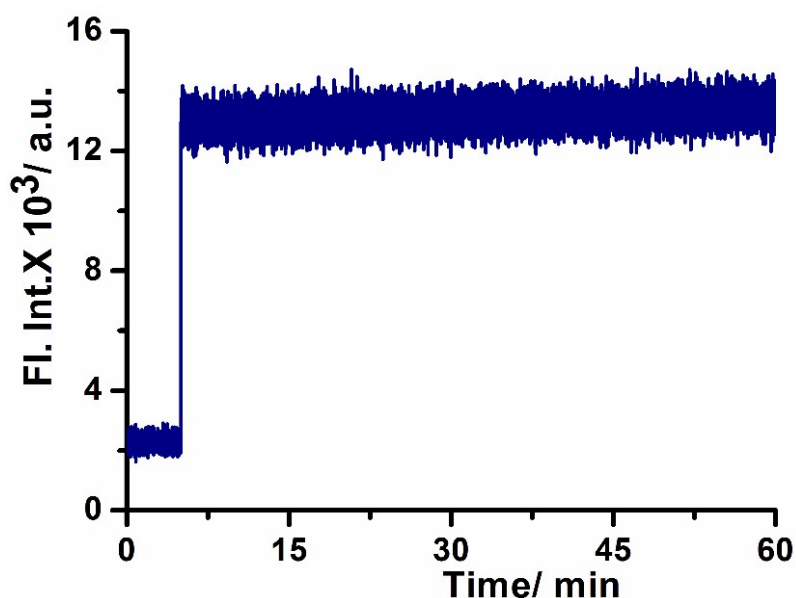


**Fig. S1** Photostability and thermal stability of PMISS: Kinetic monitoring of fluorescence intensity of PMISS in toluene at higher temperature (338 K) under continuous irradiation of light using 450 W xenon lamp in fluorolog setup with 3/3 nm excitation/emission slit width.

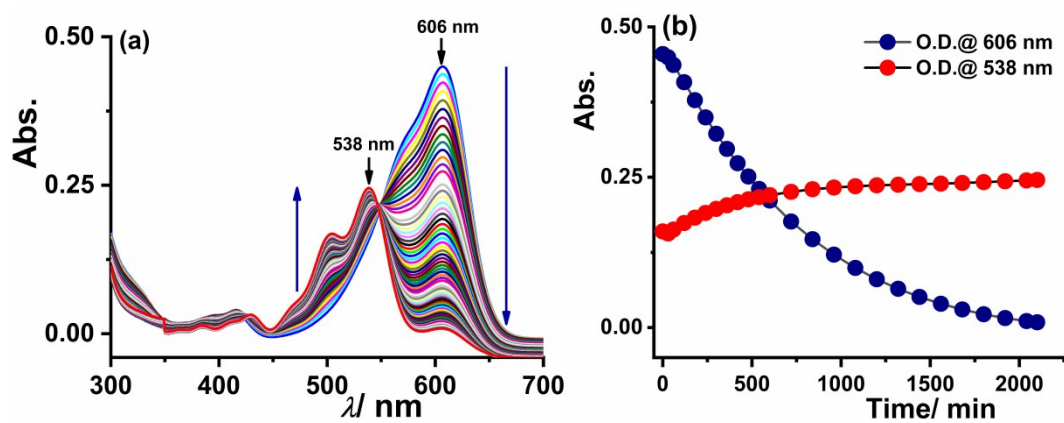


**Fig. S2** (a) Time-dependent absorption spectra of PMISS with BPO in toluene at RT (298 K), spectra were taken between 30 mins interval (b) representation of ratiometric change of O.D. with time at two wavelengths for PMISS-BPO in toluene at 298 K.

## Limit of Detection (LOD) plots:

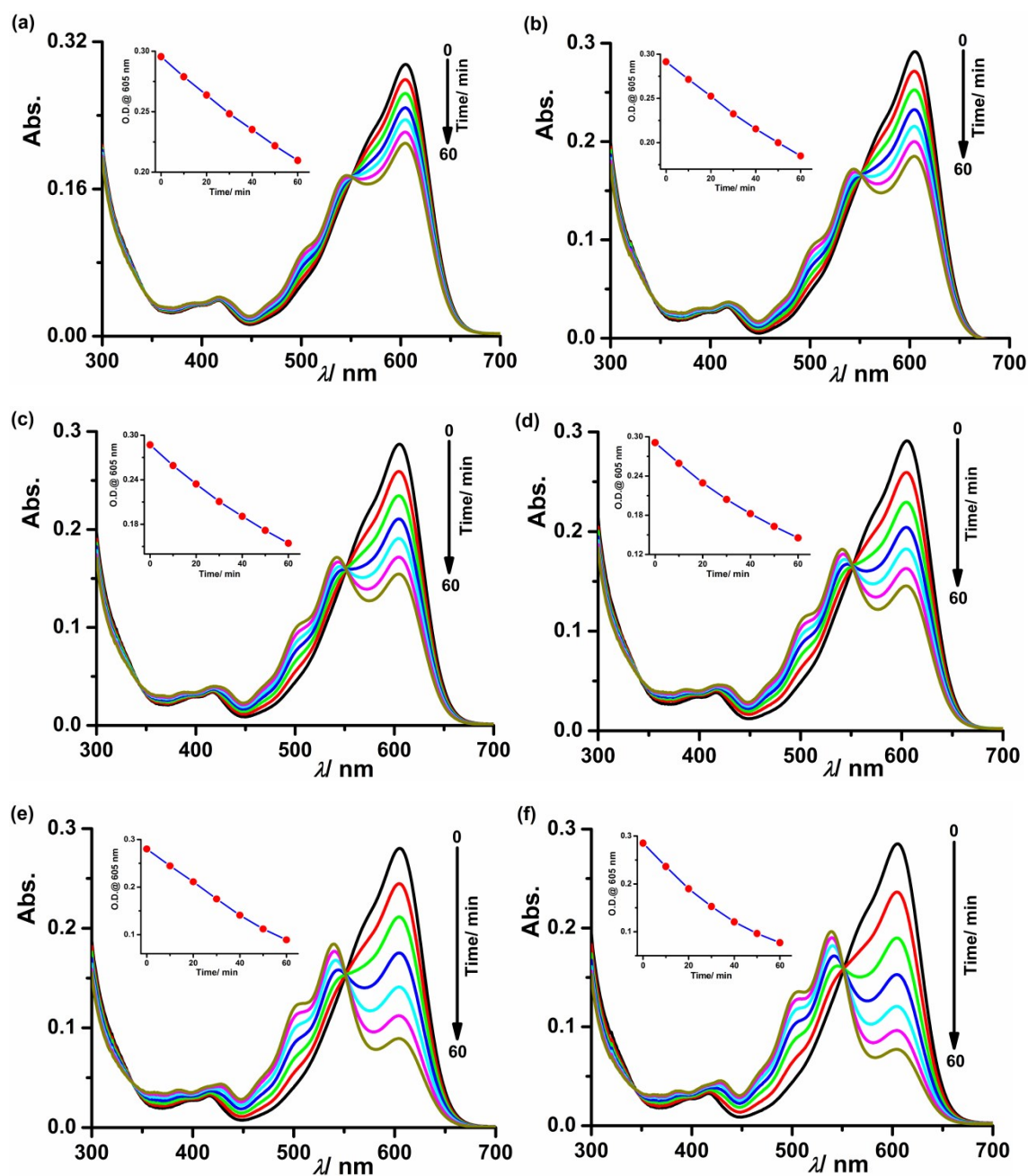


**Fig. S3** Time-dependent absorption spectra of PMISS (10  $\mu\text{M}$ ) with (a) BPO (10  $\mu\text{M}$ ), (b) BPO (20  $\mu\text{M}$ ), (c) BPO (30  $\mu\text{M}$ ), (d) BPO (40  $\mu\text{M}$ ), (e) BPO (50  $\mu\text{M}$ ), (f) BPO (75  $\mu\text{M}$ ) in toluene at 328 K, inset shows the changes of O.D. with time for different concentration of BPO.

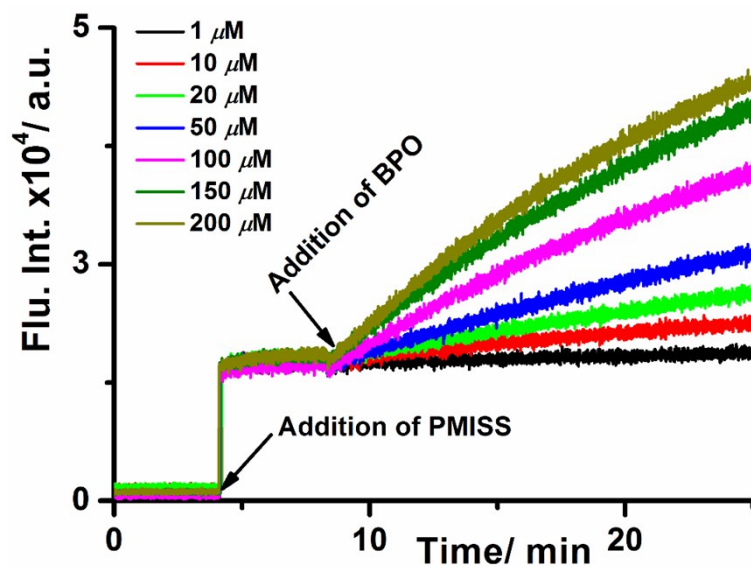


**Fig. S4** Kinetic monitoring of fluorescence of PMISS (10  $\mu\text{M}$ ) with BPO having different concentration at 338 K.

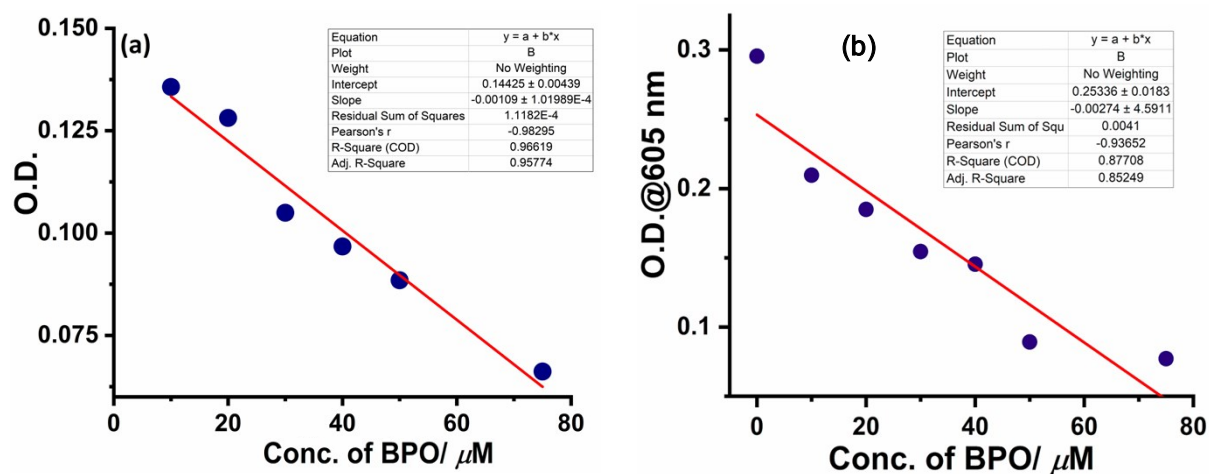


**Fig. S5** Plot of O.D. vs. concentration of BPO at (a) 298 K measured after 12 h, and (b) 328 K measured after 1 h for the determination of LOD. The LOD value is 0.28  $\mu\text{M}$  at 298 K and 0.50  $\mu\text{M}$  at 328 K.

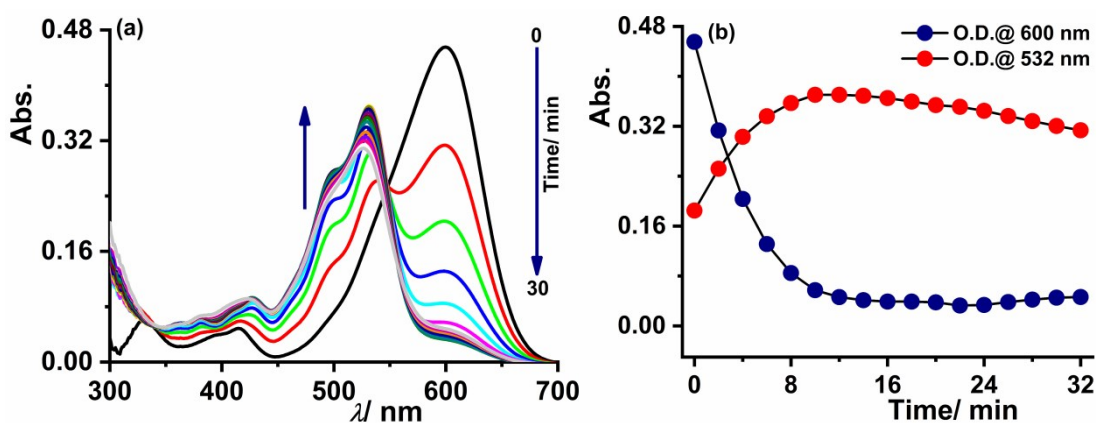


**Fig. S6** (a) Time-dependent absorption spectra of PMISS in peroxide rich (without distillation, directly taken from a year old bottle) THF at 328 K (b) representation of ratiometric change of O.D. with time at two wavelengths for PMISS in THF at 328 K

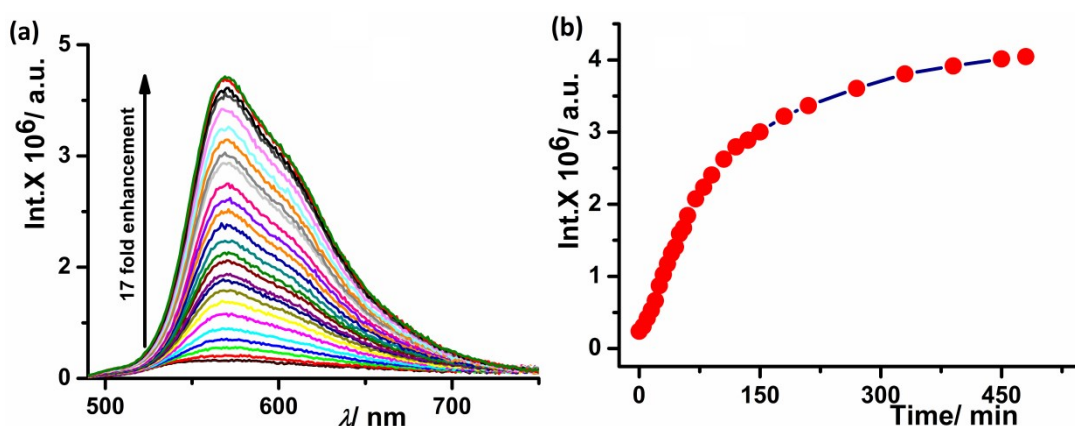


**Fig. S7** (a) Time-dependent fluorescence spectra of PMISS in peroxide rich (without distillation, taken from a year old bottle) THF at 298 K (excitation wavelength 480 nm and slit width 1.5/1.5 nm) (b) Plot of fluorescence intensity at 570 nm with time at 298 K

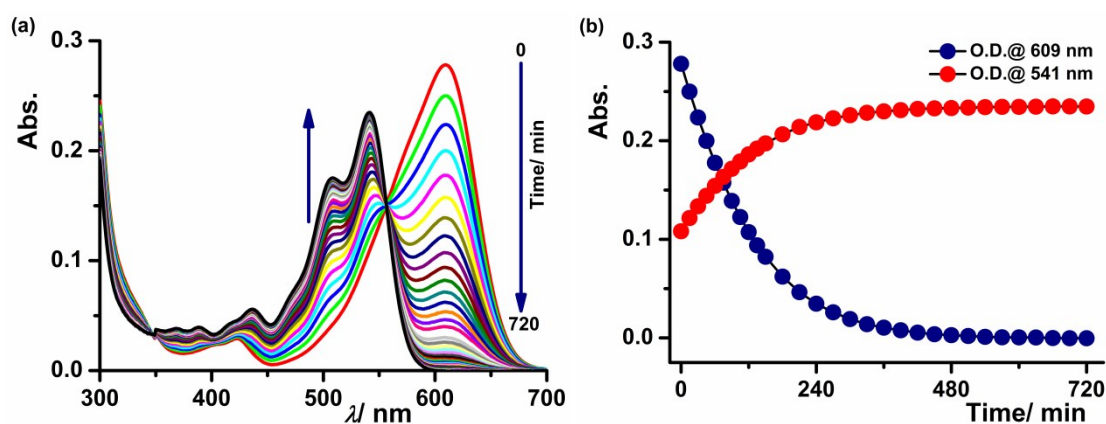


**Fig. S8** (a) Time-dependent UV-Vis. spectra of PMISS (10  $\mu$ M) in 1,4-Dioxane (without distillation, taken from an old bottle) at 298 K (b) Ratiometric plot of the time-dependent UV-Vis. spectra of PMISS (10  $\mu$ M) in 1,4-Dioxane at 298 K

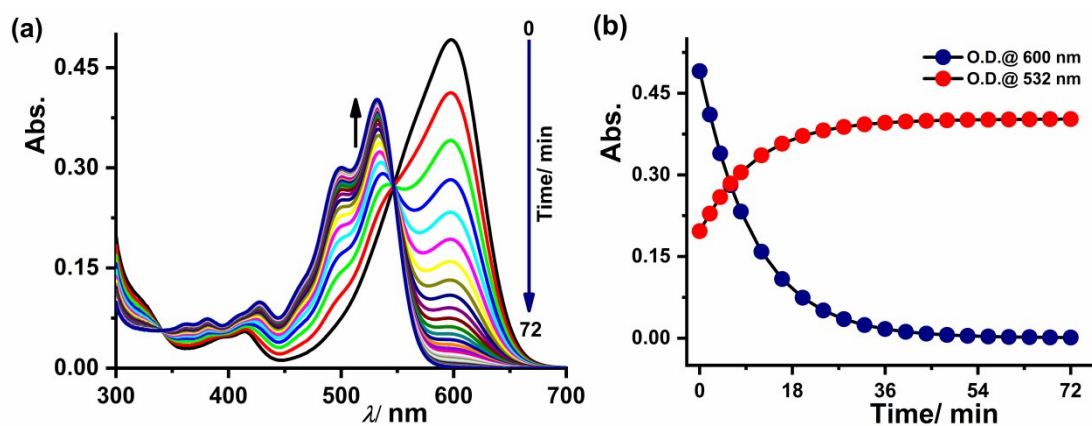


**Fig. S9** (a) Time-dependent UV-Vis. spectra of PMISS ( $10 \mu\text{M}$ ) in 1,4-dioxane (without distillation, taken from bottle) at 338 K (b) Ratiometric plot of the time-dependent UV-Vis. spectra of PMISS ( $10 \mu\text{M}$ ) in 1,4-Dioxane at 338 K

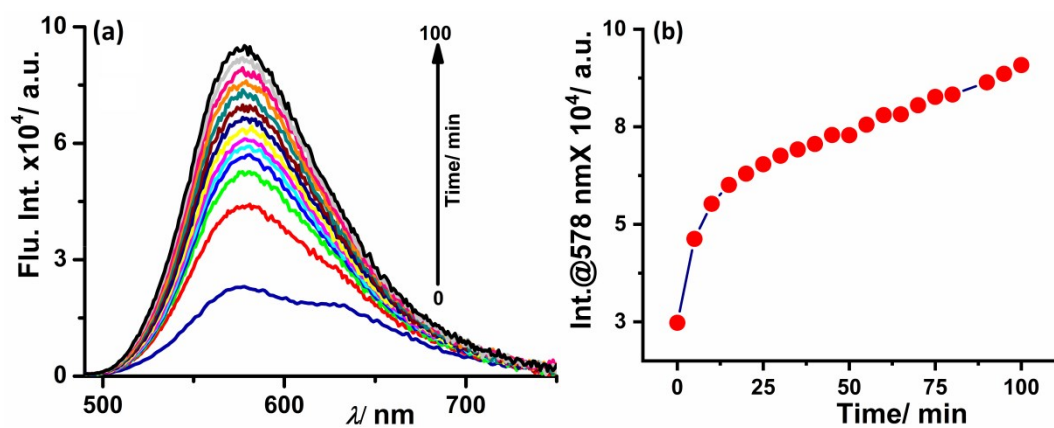


**Fig. S10** (a) Time-dependent emission spectra of PMISS ( $10 \mu\text{M}$ ) in 1,4-dioxane (without distillation, taken from bottle) at 338 K (b) Intensity at 578 nm vs. time plot of PMISS ( $10 \mu\text{M}$ ) in 1,4-dioxane at 338 K.

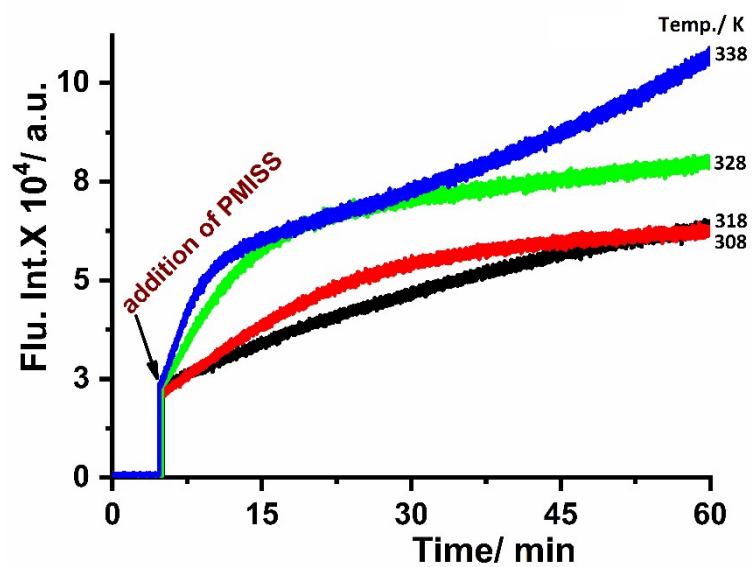


**Fig. S11** Fluorescence kinetics of PMISS ( $10 \mu\text{M}$ ) in 1,4-dioxane (without distillation, taken from an old bottle) at different temperature

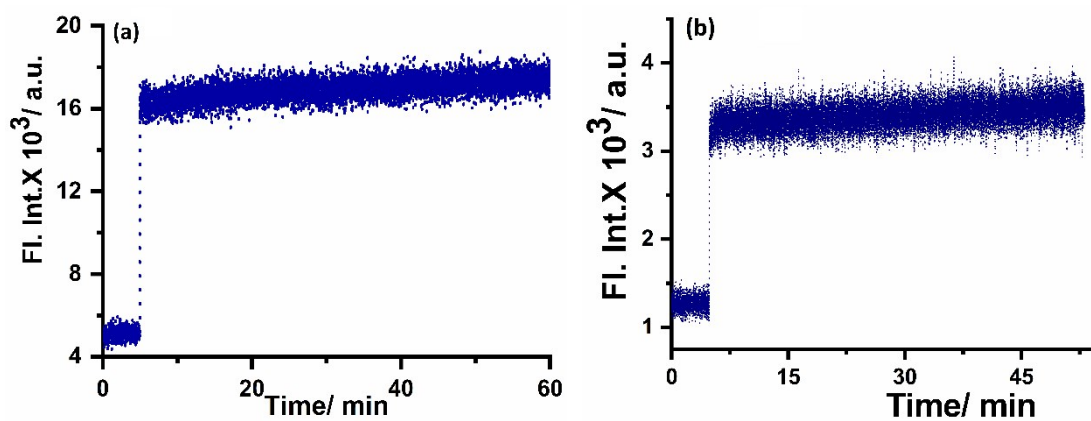


**Fig. S12** (a) Fluorescence kinetics of PMISS ( $10 \mu\text{M}$ ) in dry and distilled THF and dry and distilled 1,4-dioxane

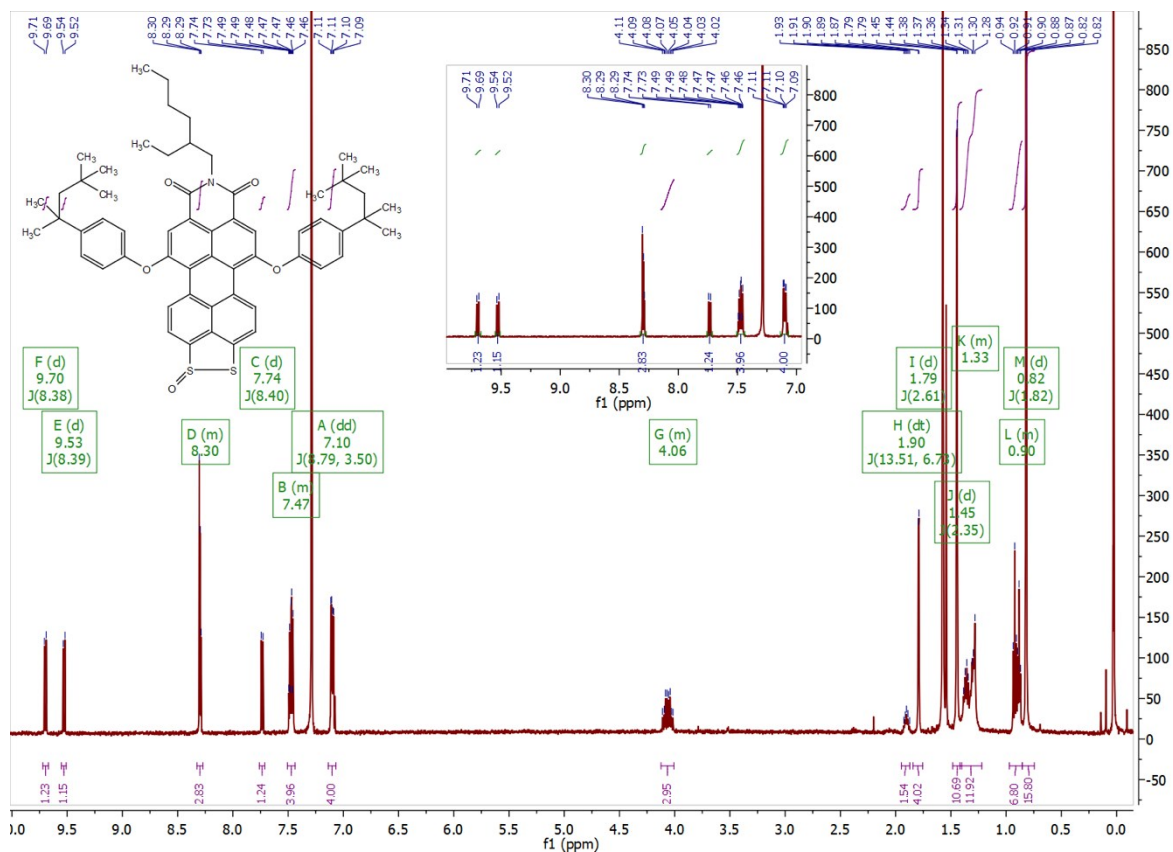


**Fig. S13** <sup>1</sup>H NMR spectrum of PMISSO derivative in CDCl<sub>3</sub> at 500 MHz

**<sup>1</sup>H NMR of PMISSO (500 MHz, Chloroform-*d*):**  $\delta$  9.70 (d,  $J = 8.4$  Hz, 1H), 9.53 (d,  $J = 8.4$  Hz, 1H), 8.32 – 8.27 (m, 3H), 7.74 (d,  $J = 8.4$  Hz, 1H), 7.47 (dd,  $J = 8.8, 6.2, 3.1$  Hz, 4H), 7.10 (dd,  $J = 8.8, 3.5$  Hz, 4H), 4.06 (m,  $J = 12.9, 7.2$  Hz, 3H), 1.90 (dt,  $J = 13.5, 6.7$  Hz, 2H), 1.79 (d,  $J = 2.6$  Hz, 4H), 1.45 (d,  $J = 2.4$  Hz, 11H), 1.42 – 1.22 (m, 12H), 0.90 (m,  $J = 18.7, 7.1$  Hz, 7H), 0.82 (d,  $J = 1.8$  Hz, 16H).

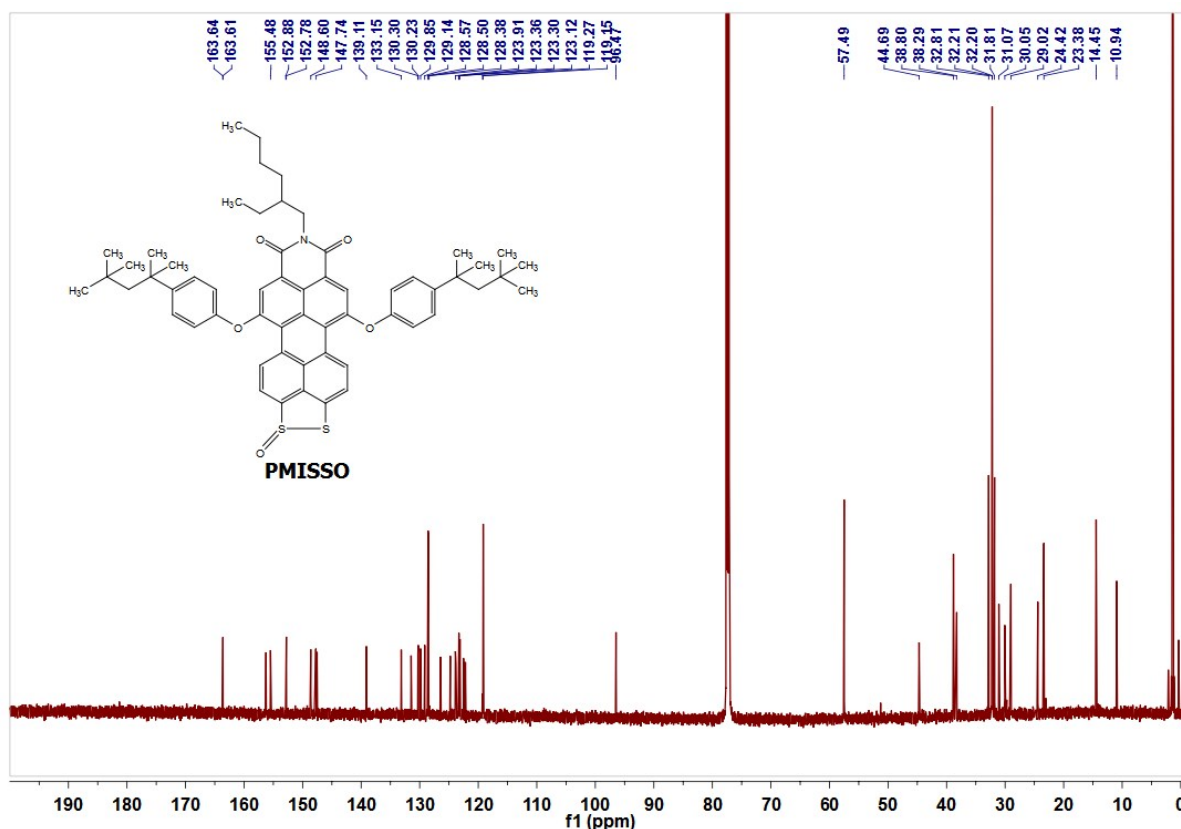


**Fig. S14**  $^{13}\text{C}$  NMR spectrum of PMISSO derivative in  $\text{CDCl}_3$

**$^{13}\text{C}$  NMR of PMISSO (176 MHz, Chloroform-*d*):**  $\delta$  163.64, 163.61, 156.26, 155.48, 152.88, 152.78, 148.60, 147.74, 147.53, 139.11, 133.15, 131.46, 130.30, 130.23, 129.85, 129.14, 128.57, 128.50, 128.38, 126.43, 124.78, 123.91, 123.80, 123.36, 123.30, 123.12, 122.51, 122.19, 119.27, 119.15, 96.47, 57.49, 44.69, 38.80, 38.29, 32.81, 32.21, 32.20, 31.81, 31.07, 30.05, 29.02, 24.42, 23.38, 14.45, 10.94.

**Acquisition Parameter**

Source Type	APCI	Ion Polarity	Positive	Set Nebulizer	2.5 Bar
Focus	Not active	Set Capillary	4000 V	Set Dry Heater	200 °C
Scan Begin	50 m/z	Set End Plate Offset	-500 V	Set Dry Gas	4.0 l/min
Scan End	3000 m/z	Set Collision Cell RF	600.0 Vpp	Set Divert Valve	Waste

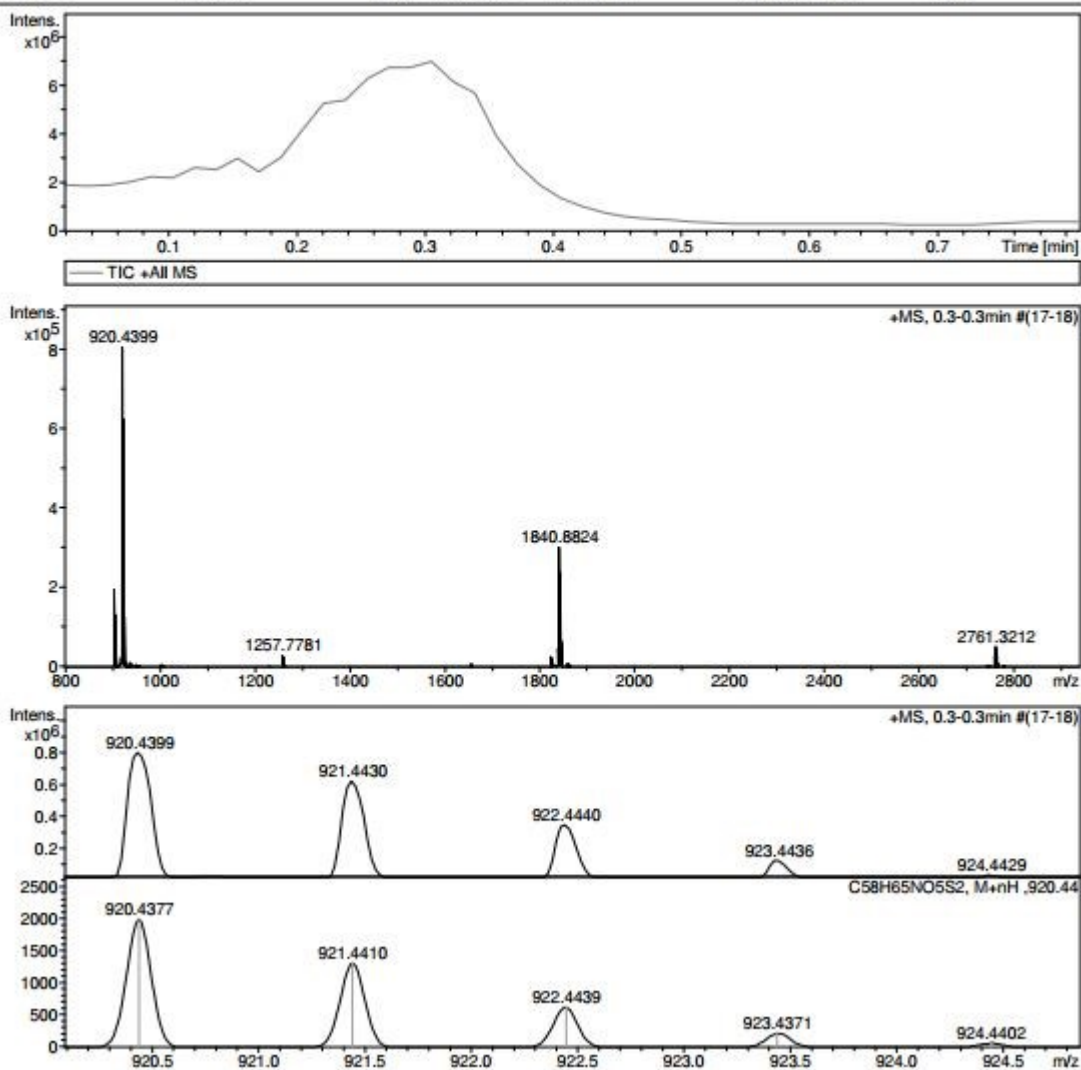


**Fig. S15** APCI mass spectrum of PMISSO

Calculated mass – 919.4304 and Obtained mass –  $m/z$  920.4399 [M+H]<sup>+</sup>

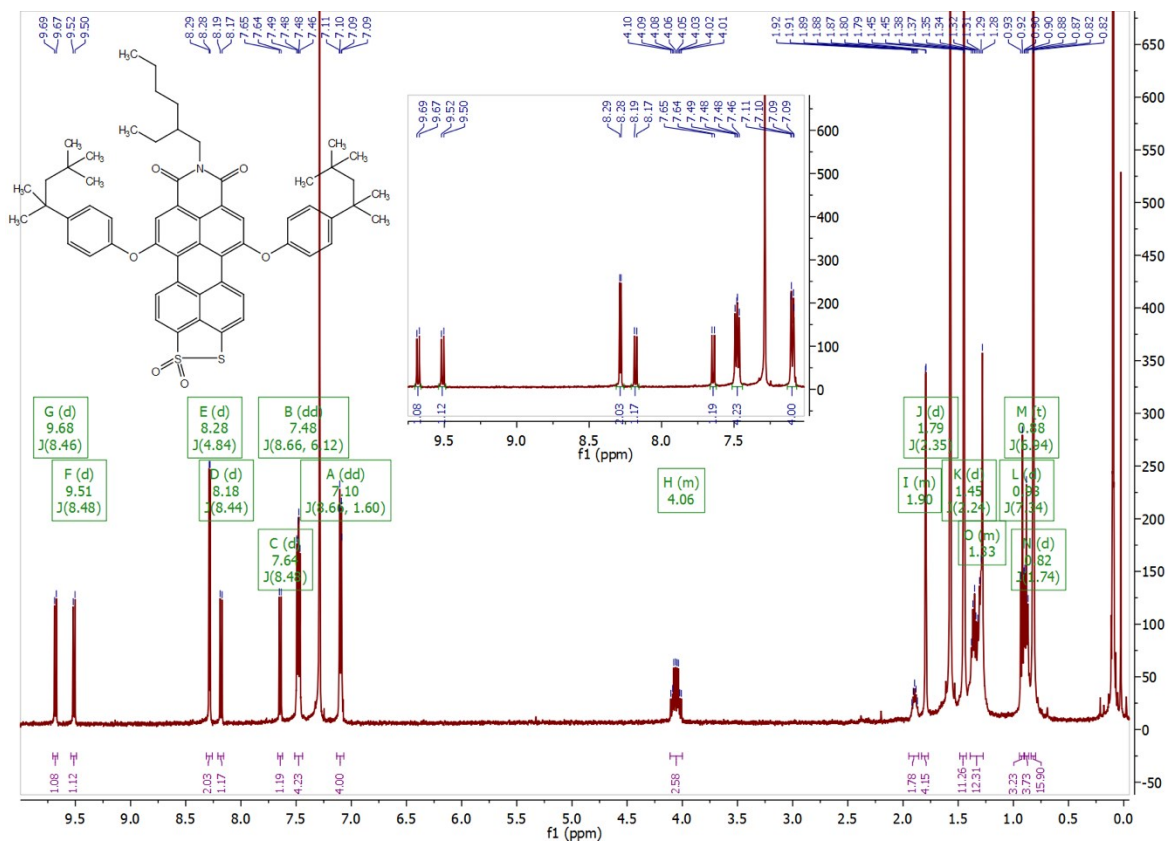


**Fig. S16** <sup>1</sup>H NMR spectrum of PMISSO<sub>2</sub> derivative in CDCl<sub>3</sub> at 500 MHz

**<sup>1</sup>H NMR of PIMSSO<sub>2</sub> (500 MHz, Chloroform-*d*):**  $\delta$  9.68 (d,  $J$  = 8.5 Hz, 1H), 9.51 (d,  $J$  = 8.5 Hz, 1H), 8.28 (d,  $J$  = 4.8 Hz, 2H), 8.18 (d,  $J$  = 8.4 Hz, 1H), 7.64 (d,  $J$  = 8.5 Hz, 1H), 7.48 (dd,  $J$  = 8.7, 6.1 Hz, 4H), 7.10 (dd,  $J$  = 8.7, 1.6 Hz, 4H), 4.06 (m,  $J$  = 19.8, 13.0, 7.2 Hz, 3H), 1.90 (m,  $J$  = 12.2, 5.8 Hz, 2H), 1.79 (d,  $J$  = 2.4 Hz, 4H), 1.45 (d,  $J$  = 2.2 Hz, 11H), 1.33 (m,  $J$  = 29.0, 13.8, 6.8 Hz, 12H), 0.93 (d,  $J$  = 7.3 Hz, 3H), 0.88 (t,  $J$  = 6.9 Hz, 4H), 0.82 (d,  $J$  = 1.7 Hz, 16H).

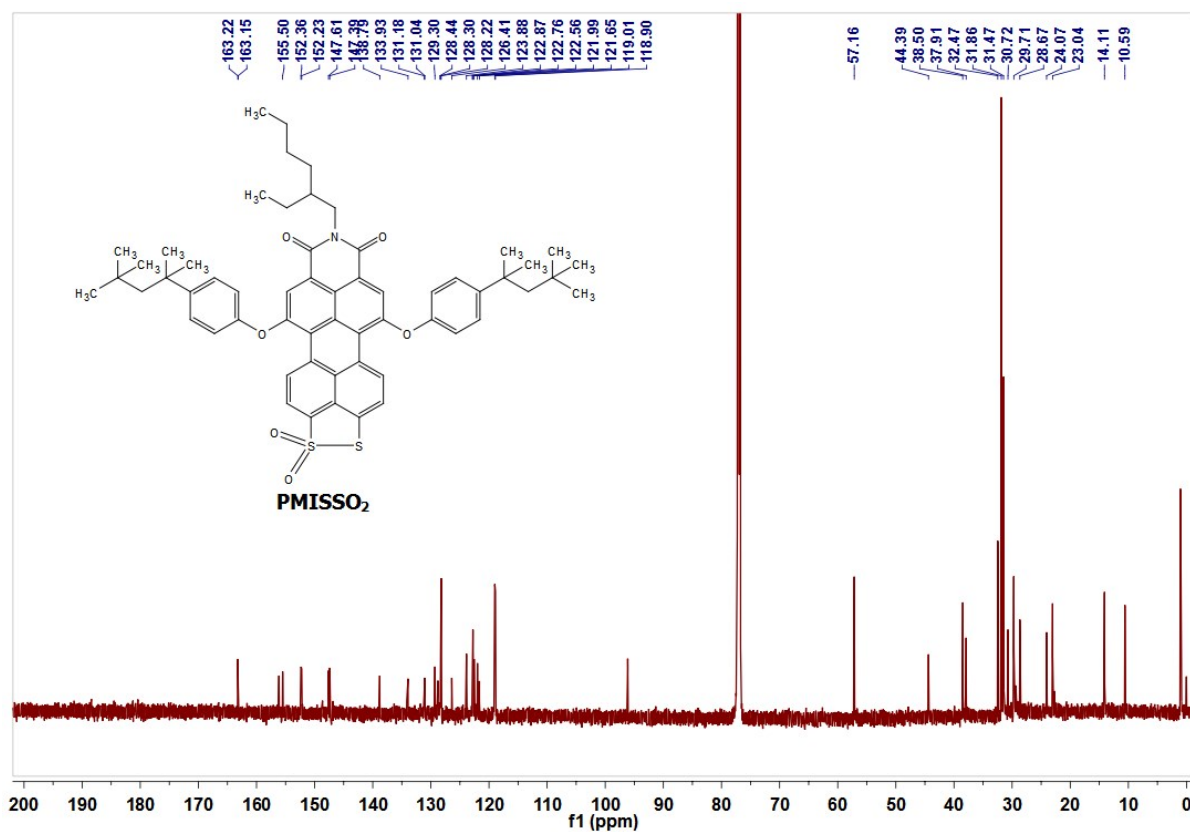


**Fig. S17** <sup>13</sup>C NMR spectrum of PMISSO<sub>2</sub> derivative in CDCl<sub>3</sub>

**<sup>13</sup>C NMR of PIMSSO<sub>2</sub> (176 MHz, Chloroform-*d*):**  $\delta$  163.22, 163.15, 156.14, 155.50, 152.36, 152.23, 147.61, 147.39, 138.79, 133.93, 131.18, 131.04, 129.30, 128.44, 128.30, 128.22, 126.41, 123.88, 122.87, 122.76, 122.56, 121.99, 121.65, 119.01, 118.90, 57.16, 44.39, 38.50, 37.91, 32.47, 31.86, 31.47, 30.72, 29.71, 28.67, 24.07, 23.04, 14.11, 10.59.

**Acquisition Parameter**

Source Type	APCI	Ion Polarity	Positive	Set Nebulizer	2.5 Bar
Focus	Not active	Set Capillary	4000 V	Set Dry Heater	200 °C
Scan Begin	50 m/z	Set End Plate Offset	-500 V	Set Dry Gas	4.0 l/min
Scan End	3000 m/z	Set Collision Cell RF	600.0 Vpp	Set Divert Valve	Waste

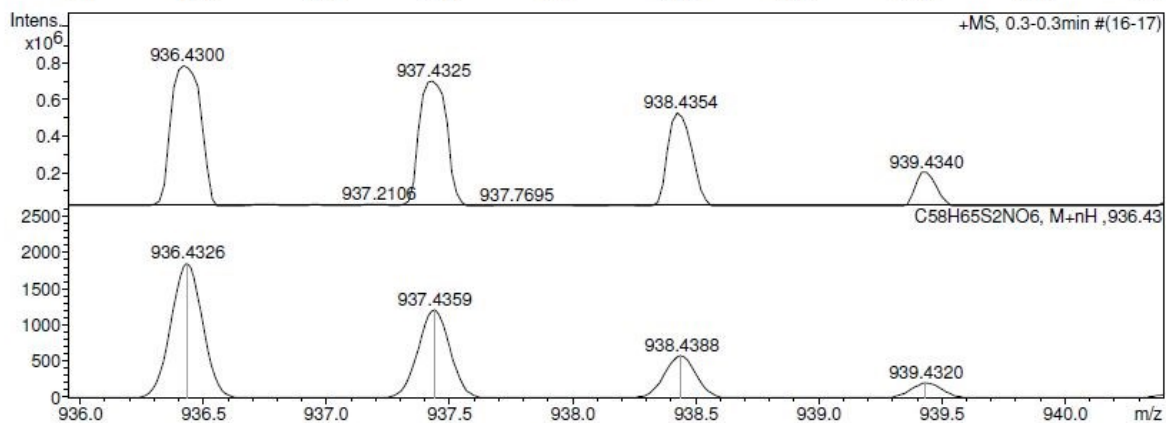
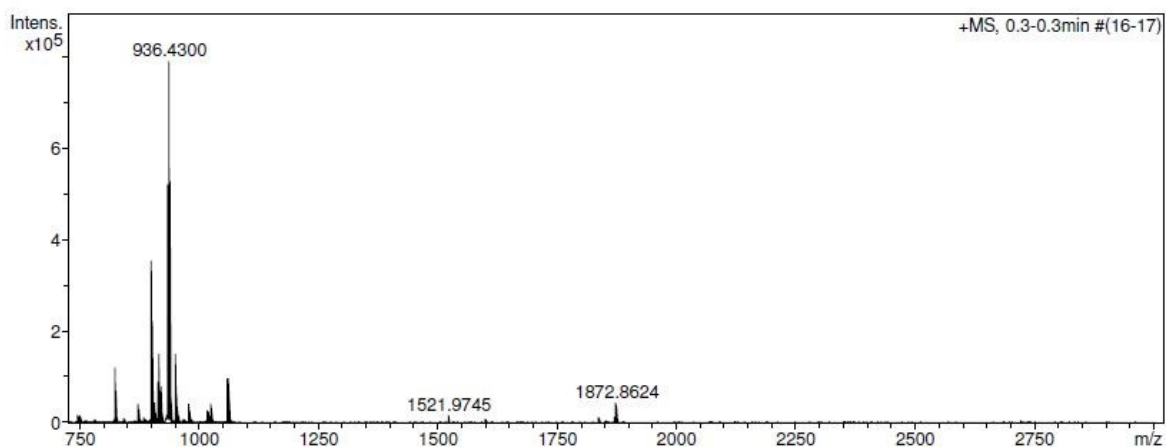
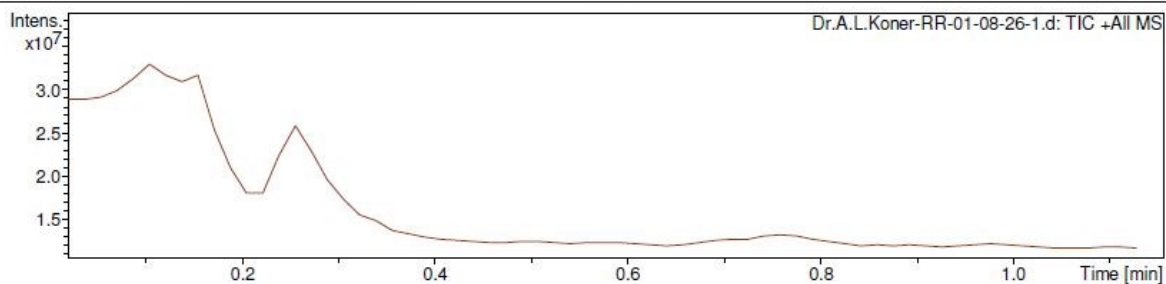


**Fig. S18** APCI mass spectrum of PMISSO<sub>2</sub>

**Calculated mass – 935.4253 and Obtained mass –  $m/z$  936.4300 [M+H]<sup>+</sup>**

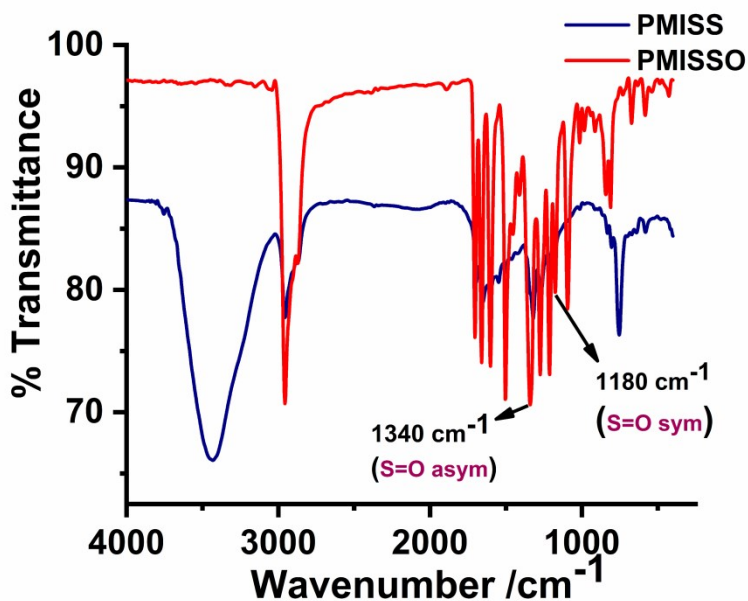


Fig. S19 Merged IR spectra of PMISS and PMISSO for confirmation of oxidized species

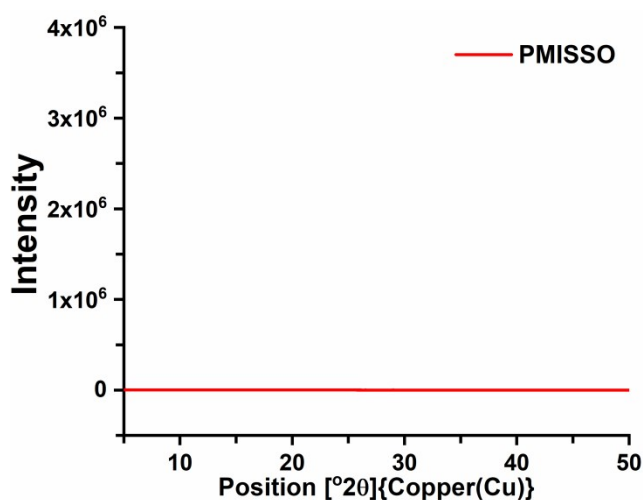


Fig. S20 Powder X-Ray Diffraction (PXRD) pattern of PMISSO powder showing absence of diffraction peaks indicating its amorphous nature.

**SCXRD.** Single crystals of  $\text{PMISSO}_2$  suitable for X-Ray diffraction analysis were obtained by slow evaporation method from a solvent mixture of dichloromethane, *N,N*-dimethylformamide and hexane kept at low temperature ( $4^\circ\text{C}$ ). Single Crystal X-ray Diffraction data were collected on Bruker *AXS Kappa APEXII* diffractometer using monochromatic  $\text{Mo K}\alpha$  radiation ( $\lambda = 0.71073 \text{ \AA}$ ) at 100 K using an Oxford Cryostream low-temperature device. Unit cell measurement, data integration, scaling and absorption correction for the crystal were done with Bruker *APEXII* software.<sup>4</sup> Data reduction was carried out with Bruker *S SAINT* suite.<sup>5</sup> Absorption correction was performed by multi-scan method implemented in *SADABS*.<sup>6</sup> The crystal structure was solved by direct methods using *SIR 2014*.<sup>7</sup> The crystal structure

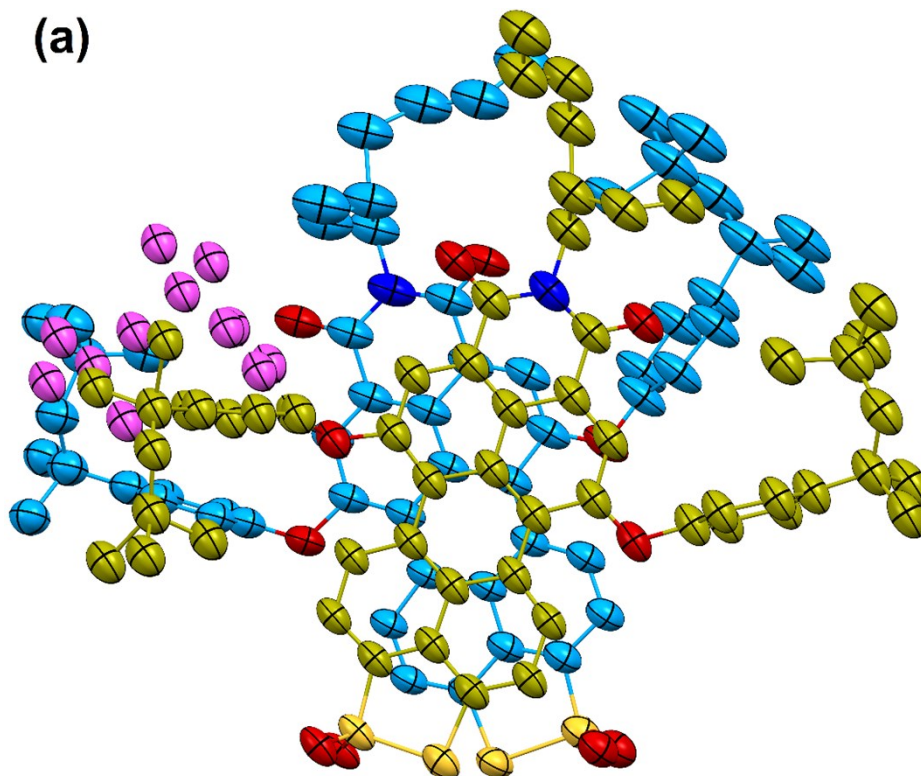
refinement was performed in the program package *OLEX2*,<sup>8</sup> and all non-hydrogen atoms were refined anisotropically by full matrix least-squares calculations based on  $F^2$  using *SHELXL-2018*.<sup>9</sup> All the hydrogen atoms were positioned geometrically and refined using a riding model. Details of crystal data, data collection, and refinement details are given in Table S1. Geometrical calculations were carried out using *PARST*<sup>10</sup> and *PLATON*.<sup>11</sup> *MERCURY*<sup>12</sup> program was used for structure analysis and for preparation of molecular and crystal structure diagrams.

**Table S1.** Crystal Data and Structure Refinement

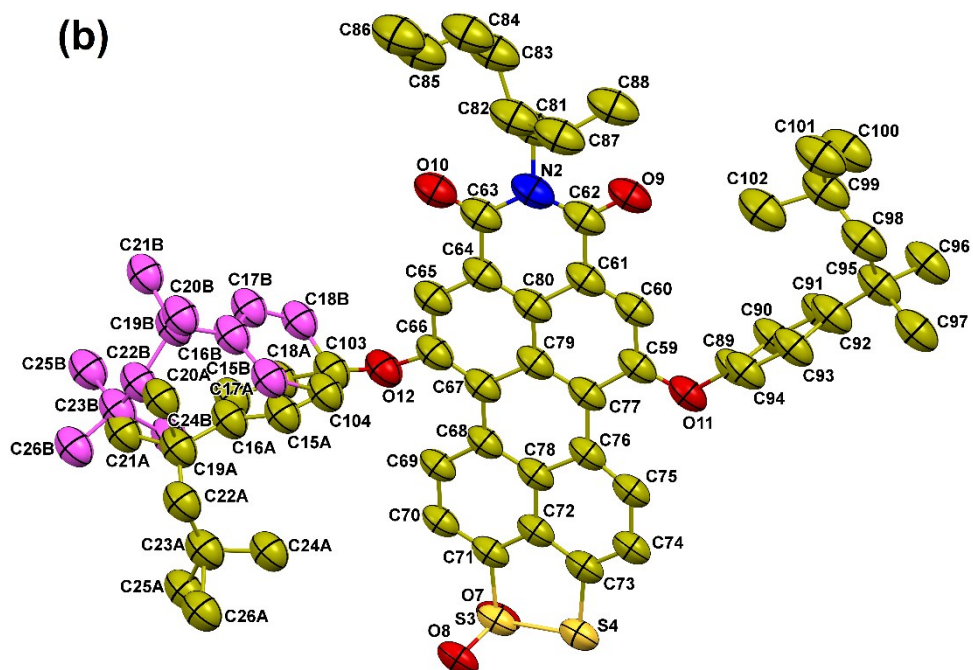
Sample Code	PMISSO <sub>2</sub>
Formula	C <sub>58</sub> H <sub>65</sub> N O <sub>6</sub> S <sub>2</sub>
Solvent	DCM + DMF + Hexane
Crystal Size (mm)	0.15 X 0.08 X 0.06
Morphology	Block
Formula Weight	936.23
Temperature (K)	100 (2)
Wavelength (Å)	0.71073
Crystal System	Monoclinic
Space Group	$P\bar{1}$
Z, Z <sub>□</sub>	4, 2
a (Å)	12.0522(6)
b (Å)	17.6311(11)
c (Å)	25.4763(15)
α (°)	71.449(4)
β (°)	81.456(4)
γ (°)	83.555(4)
Volume (Å <sup>3</sup> )	5063.1(5)
Density (g cm <sup>-3</sup> )	1.228
F (000), μ(mm <sup>-1</sup> )	2000, 0.157
θ (min, max) (°)	0.849, 25.026
h <sub>min,max</sub> , k <sub>min,max</sub> , l <sub>min,max</sub>	(-13,14), (-20,19), (-30,30)
Treatment of Hydrogens	Fixed
No. unique ref/obs. Ref.	17072, 6560
No of Parameters	1317
R <sub>all</sub> , R <sub>obs</sub>	0.3338, 0.2022
wR <sub>2_all</sub> , wR <sub>2_obs</sub>	0.5573, 0.4997

$\Delta\rho_{\min,\max}(\text{e}\text{\AA}^{-3})$	-1.023, 1.736
G.O.F	1.633
CCDC	1994672

(a)



(b)



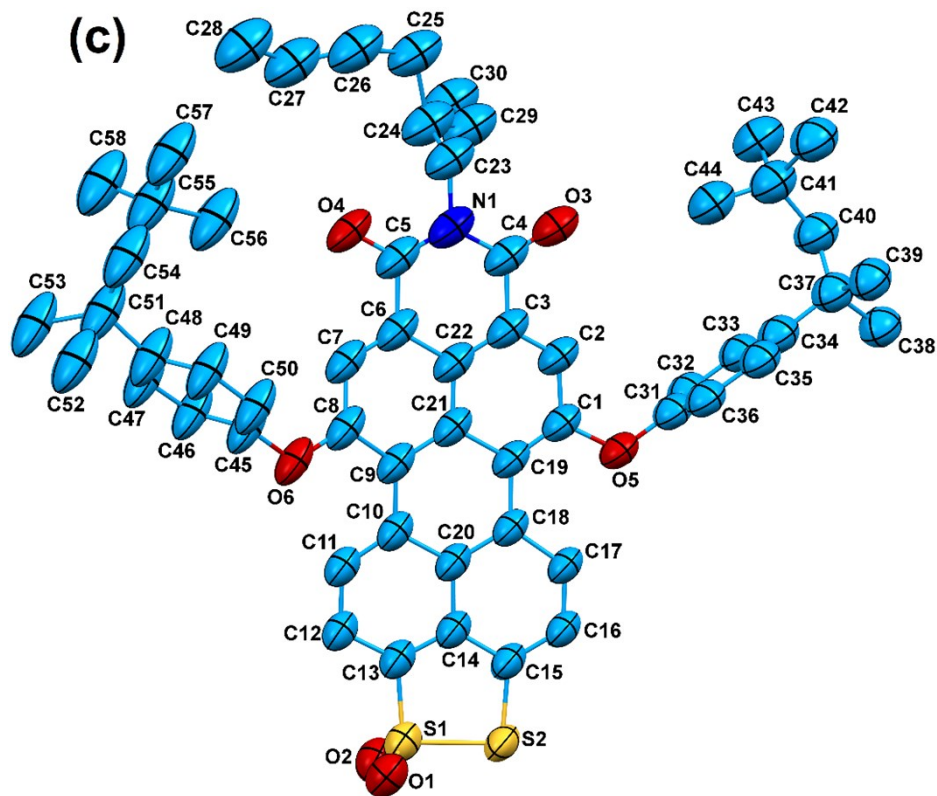


**Fig. S21** (a) ORTEP of PMISSO<sub>2</sub> showing two molecules depicted by golden and blue coloured carbon atoms in the asymmetric unit of the unit cell. (b) ORTEP of the golden colour PMISSO<sub>2</sub> molecule which exhibits a two-component dynamic disorder with a 51:49 disorder ratio in one of the 4-tert-octylphenoxy fragment (disordered component shown in pink colour) at one of 1,6-bay position. (b) ORTEP of the blue coloured PMISSO<sub>2</sub> molecule. All the ellipsoids are drawn at 50 % probability level and hydrogen atoms have been omitted for clarity.

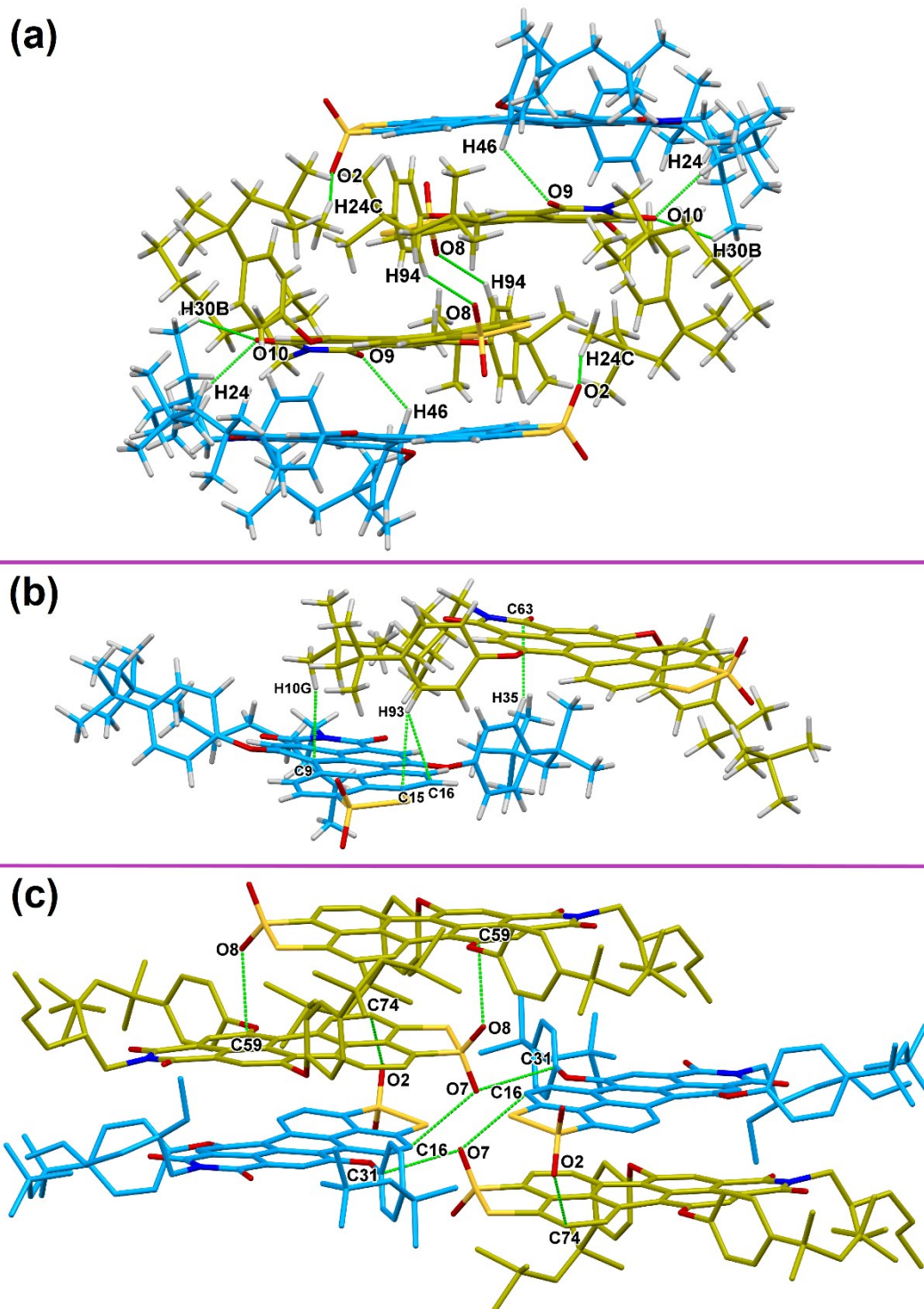


**Fig. S22** (a) C–H $\cdots$ O hydrogen bonding interactions between SO<sub>2</sub> and 1,6-bay substituted 4-tert-octylphenoxide moieties prevent  $\pi\cdots\pi$  stacking interactions between gold coloured molecules, but are present only between blue and gold coloured PMISSO<sub>2</sub> molecules, (b) C–H $\cdots\pi$  interactions between parallel displaced PMISSO<sub>2</sub> molecules of two neighbouring columns (c) O(*lp*) $\cdots\pi$  interactions between SO<sub>2</sub> moiety and perylene core preventing  $\pi\cdots\pi$  interactions between gold coloured PMISSO<sub>2</sub> molecules. O(*lp*) $\cdots\pi$  interactions forming a

tetramer between PMISSO<sub>2</sub> molecules belonging to adjacent columns. Hydrogen atoms have been removed for clarity.

**Table S2.** Intermolecular Hydrogen bonds, C–H $\cdots\pi$ ,  $\pi\cdots\pi$  and O(*lp*) $\cdots\pi$  interactions in PMISSO<sub>2</sub> crystals.

Intermolecular Interactions	Symmetry Code	H $\cdots$ A (Å)	D $\cdots$ A (Å)	D–H $\cdots$ A (°)
C94–H94 $\cdots$ O8	1-x, 1-y, 1-z	2.56	3.364(3)	143
C87–H87A $\cdots$ O3	-1+x, y, z	2.57	3.529(4)	162
C24–H24 $\cdots$ O10	x, y, z	2.28	3.159(4)	146
C30–H30B $\cdots$ O10	x, y, z	2.57	3.352(4)	136
C25A–H25A $\cdots$ O1	x, 1+y, z	2.40	3.361(3)	140
C24A–H24C $\cdots$ O2	1-x, 1-y, 1-z	2.50	3.380(3)	149
C35–H35 $\cdots$ C63( $\pi$ )	-1+x, y, z	2.82	3.701(2)	155
C93–H93 $\cdots$ C16( $\pi$ )	-1+x, y, z	2.82	3.518(2)	131
C93–H93 $\cdots$ C15( $\pi$ )	-1+x, y, z	2.82	3.697(2)	153
C101–H10G $\cdots$ C9( $\pi$ )	-1+x, y, z	2.79	3.741(2)	163
C68( $\pi$ ) $\cdots$ C18( $\pi$ )	x, y, z		3.497(2)	
C68( $\pi$ ) $\cdots$ C19( $\pi$ )	x, y, z		3.422(2)	
C67( $\pi$ ) $\cdots$ C21( $\pi$ )	x, y, z		3.431(2)	
C59( $\pi$ ) $\cdots$ C11( $\pi$ )	x, y, z		3.381(2)	
C77( $\pi$ ) $\cdots$ C10( $\pi$ )	x, y, z		3.451(2)	
C69( $\pi$ ) $\cdots$ C1( $\pi$ )	x, y, z		3.424(2)	
C64( $\pi$ ) $\cdots$ C6( $\pi$ )	x, y, z		3.423(2)	
C63( $\pi$ ) $\cdots$ C5( $\pi$ )	x, y, z		3.475(2)	
O8( <i>lp</i> ) $\cdots$ C59( $\pi$ )	1-x, 1-y, 1-z		3.053(1)	
O7( <i>lp</i> ) $\cdots$ C16( $\pi$ )	x, y, z		3.131(2)	
O2( <i>lp</i> ) $\cdots$ C74( $\pi$ )	x, y, z		3.153(1)	
O7( <i>lp</i> ) $\cdots$ C31( $\pi$ )	2-x, 1-y, 1-z		3.162(1)	

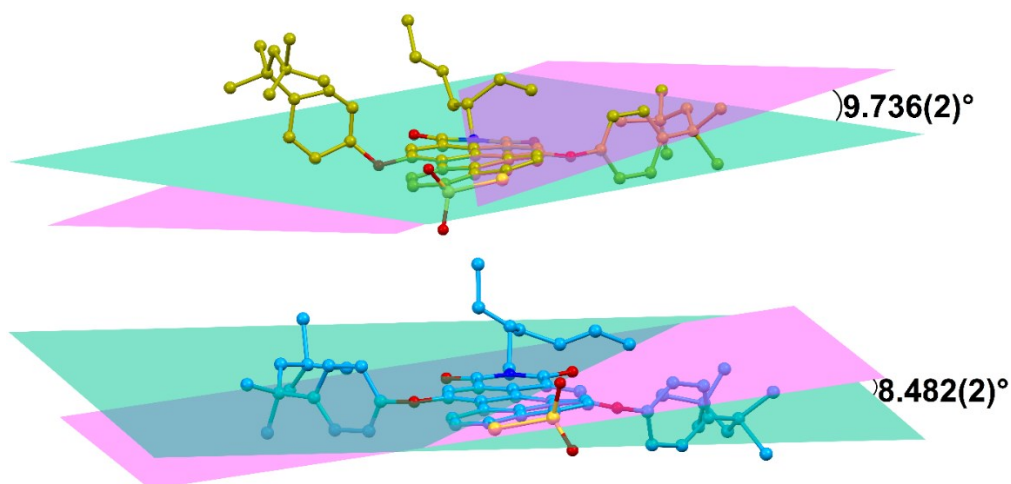


**Fig. S23** Twist angles of 9.736(2)° and 8.482(2)° between the mean planes of the naphthalene rings (indicated by pink and cyan colours) in the two PMISSO<sub>2</sub> molecules of the asymmetric unit depicting their perylene core distortion. Hydrogen atoms have been omitted for clarity

**Solvent-dependent absorption spectra of PMISSO<sub>2</sub>:** The experimental UV-vis. absorption spectra of PMISSO<sub>2</sub> recorded in various solvents like Chloroform (CHCl<sub>3</sub>), Toluene, 1,4-dioxane and Tetrahydrofuran (THF) are shown in **Figure S22**. The general features of the absorption spectra of PMISSO<sub>2</sub> are very similar suggesting that the electronic structure of the boundary orbitals is very slightly affected by changing the polarity of the solvent.

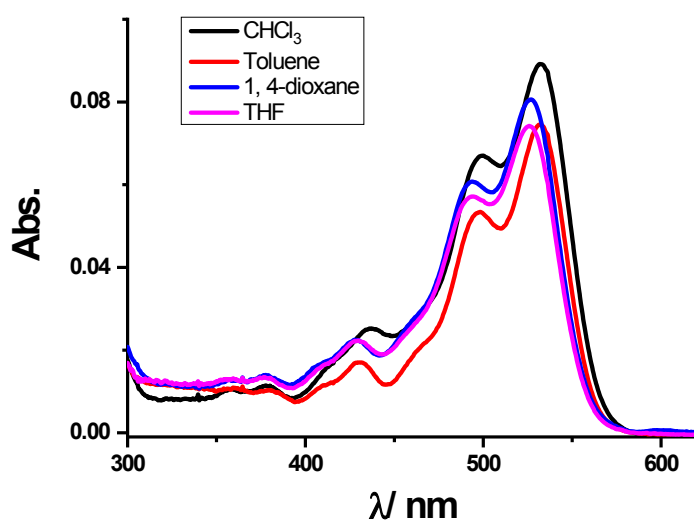


**Fig. S24** Experimental UV-vis. absorption spectra of PMISSO<sub>2</sub> recorded in CHCl<sub>3</sub>, Toluene, 1,4-dioxane and THF solvents measured at 298 K.

In order to correlate the molecular electronic structure with the UV-Vis experimental band positions, the crystal geometry of PMISSO<sub>2</sub> has been optimized at the B3LYP/6-311G(d,p) level of theory in CHCl<sub>3</sub>, Toluene and THF solvents, including solvent polarizability by employing Polarizable Continuum Model (PCM) using the integral equation formalism variant (IEFPCM) of SCRF method. The electronic transitions of PMISSO<sub>2</sub>, calculated by Time Dependent Density Functional Theory (TD-DFT)/B3LYP/6-311G(d,p) level of theory in CHCl<sub>3</sub>, Toluene and THF solvents are compared with the experimental bands in Table S3. The most intense experimental band of PMISSO<sub>2</sub> ranging between 526-532 nm in all the solvents are almost fully reproduced in both intensity and wavelength by TD-DFT computations.

**Table S3.** Comparison of experimental UV-vis absorption spectra with calculated via-TDDFT method of PMISSO<sub>2</sub> in polar solvent medium.

Solvent	Experimental $\lambda_{\max}$ (nm)	TDDFT $\lambda_{\max}$ (nm)	Orbitals involved in transition	$\Delta E_{\text{transition}}$ (eV)	Oscillator strength ( $f$ )	Transition Dipole Moment (D)	Transition Probability (%)
CHCl <sub>3</sub>	532	543	HOMO-1 $\rightarrow$ LUMO	2.28	0.69	12.36	79
Toluene	531	533	HOMO-1 $\rightarrow$ LUMO	2.33	0.63	11.04	68
THF	526	548	HOMO-1 $\rightarrow$ LUMO	2.26	0.71	12.82	83

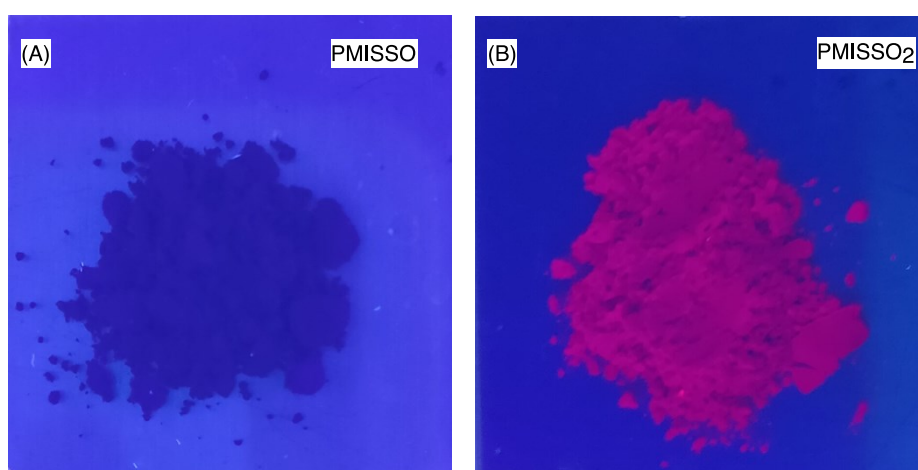


**Fig. S25** Digital photograph of the powder of (A) PMISSO and (B) PMISSO<sub>2</sub> mixed with BaSO<sub>4</sub> under 365 nm UV light. PMISSO is completely non-fluorescent whereas PMISSO<sub>2</sub> shows strong solid-state fluorescence as evident from the picture.

## References:

1. Sahoo, D.; Sharma, V.; Roy, R.; Varghese, N.; Mohanta, K.; Koner, A. L., Synthesis of highly-soluble push-pull perylenemonoimide derivatives by regioselective perifunctionalization for switchable memory applications. *Chem. Commun.* **2019**, *55* (1), 103-106.
2. Tomizaki, K.-Y.; Loewe, R. S.; Kirmaier, C.; Schwartz, J. K.; Retsek, J. L.; Bocian, D. F.; Holten, D.; Lindsey, J. S., Synthesis and Photophysical Properties of Light-Harvesting Arrays Comprised of a Porphyrin Bearing Multiple Perylene-Monoimide Accessory Pigments. *J. Org. Chem.* **2002**, *67* (18), 6519-6534.
3. CIE(1931). *Commission internationale de l'Eclairage proceedings*, 1931. Cambridge: Cambridge University Press
4. V. U. M. Apex2, M86-E01078, Bruker Analytical X-ray Systems Madison, WI, **2006**.
5. S. S. Siemens, Siemens Analytical X-ray Instruments Inc. Madison, MI, **1995**.
6. G. M. S. B. A. Sheldrick, Inc.: Madison, WI, 2007.
7. M. C. Burla, R. Caliendo, B. Carrozzini, G. L. Cascarano, C. Cuocci, C. Giacovazzo, M. Mallamo, A. Mazzone, G. Polidori, *J. Appl. Cryst.* **2015**, *48*, 306–309.
8. O. V. Dolomanov, L. J. Bourhis, R. J. Gildea, J. A. K. Howard, H. Puschmann *J. Appl. Cryst.* **2009**, *42*, 339–341.
9. G. Sheldrick, *Acta Cryst. C* **2015**, *71*, 3–8.
10. M. Nardelli, *J. Appl. Cryst.* **1995**, *28*, 659.
11. A. Spek, *Acta Crystallogr. D* **2009**, *65*, 148–155.
12. C. F. Macrae, I. J. Bruno, J. A. Chisholm, P. R. Edgington, P. McCabe, E. Pidcock, L. Rodriguez-Monge, R. Taylor, J. van de Streek, P. A. Wood, *J. Appl. Cryst.* **2008**, *41*, 466–470.